(This is a sample cover image for this issue. The actual cover is not yet available at this time.)

Journal of Manufacturing Systems 54 (2020) 35–49

Contents lists available at ScienceDirect

Journal of Manufacturing Systems

journal homepage: www.elsevier.com/locate/jmansys

Circular and cylindrical profile monitoring considering spatial correlations

Chen Zhao[a], Shichang Du[a,*], Yafei Deng[a], Guilong Li[a], Delin Huang[b]

[a] Department of Industrial Engineering and Management, School of Mechanical Engineering, Shanghai Jiao Tong University, Shanghai, 200240, China
[b] College of Mechanical Engineering, Donghua University, Shanghai, 201600, China

ARTICLE INFO

Keywords:
Circular and cylindrical profiles
Statistical process control
Profile monitoring
Spatial correlations

ABSTRACT

Geometric specifications are important control objects of mechanical components in modern manufacturing. For instance, circularity and cylindricity are essential indicators of high-precision rotary parts. With an increase in the number of measurement points, traditional statistical process control (SPC) methods cannot be applied in many processes because the measurements are highly correlated. During the past two decades, several studies have focused on profile monitoring. A profile, which describes the relationship between independent and response variables, is suitable for large-scale, complex and high-dimensional data monitoring. However, the issue of spatial correlations in measurement points remains unsolved. Considering spatial correlations, this study focuses on circular and cylindrical profiles and proposes a new method combining a spatial correlation model with control charting. SPC methods are utilized to establish control charts and analyze the control processes. The results of simulation and case study indicate that the proposed method is feasible and effective in monitoring circular and cylindrical profiles and can be extended to other geometric specifications.

1. Introduction

From design, manufacturing to recycling, the tasks of geometric specifications cover the entire life cycle of the product [1]. Geometric specifications, which refer to the deviation of the actual shape of a machined part from its ideal shape, have received substantial attention in recent years, as they considerably influence the quality of mechanical components. Geometric specifications (such as circularity and cylindricity) are important control objects and particularly impact the sealing, reliability and life of products [2,3].

Statistical process control (SPC) is a common method for the control of geometric specifications. Deng and Chin [4] explored the factors affecting the circularity of a hole by using Taguchi methods. Keshteli et al. [5] proposed a method to calculate the process capability index of a circular profile. However, these methods focus only on the overall conditions of circularity and cylindricity, resulting in an inaccurate control process.

The development of measurement technology has led to an increase in the number of measurement points to provide detailed information regarding the geometric specification shapes. Under this circumstance, profile monitoring has been proposed. A profile describes the relationship between explanatory and response variables, making extensive use of measurements. Research on profile monitoring has expanded from linear [6,7] to nonlinear [8–10], unitary to multivariate [11,12], 2-D [13] to 3-D surface [14], parametric to nonparametric domains [15–17] and single channel to multichannel [18].

For circular and cylindrical profile monitoring, some methods considering the features of circular and cylindrical profiles have been proposed. Cho and Tu [19] described a harmonic decomposition method for circular profile variation. Based on this method, Jiang et al. [20] evaluated roundness from circular coordinate data measured by a coordinate measuring machine (CMM) and Zhang et al. [21] extended this method to cylindrical components. Ramaswami et al. [22] proposed a new circular feature sampling strategy to determine the optimal sample size and calculated the circular profile error by minimum circumscribed circle method. Principal component analysis [23–25] and independent component analysis [26] methods are used to separate the components of geometric specifications and analyze the causes of error. Some machine learning methods such as neural network algorithms [27] and Gaussian processes [28,29] have been proposed to detect changes in the profiles.

However, in a data-rich manufacturing environment, a large amount of data causes strong spatial correlations among measurements. Colosimo et al. [30] explored a spatial autoregressive regression (SARX) model to study the spatial correlations of error terms. Soleimani, Noorossana and Amiri [31] considered profile autocorrelation in linear

* Corresponding author.
E-mail addresses: zhao_chen@sjtu.edu.cn (C. Zhao), lovbin@sjtu.edu.cn (S. Du), phoenixdyf@sjtu.edu.cn (Y. Deng), lgl52613@sjtu.edu.cn (G. Li), huangdelin@dhu.edu.cn (D. Huang).

https://doi.org/10.1016/j.jmsy.2019.11.011
Received 18 January 2019; Received in revised form 20 November 2019; Accepted 20 November 2019

profile monitoring. They assumed that error terms are correlated and extended this correlation to observations. Yu and Liu [32] proposed a new control chart to monitor the mean shifts of autocorrelated manufacturing processes. For profiles' data violating the assumption of normal distribution, Liu et al. [29] proposed a mixed-effect profile model to monitoring wafer thickness. However, few studies have focused on the case that the observations are spatially correlated.

The composition of a geometric specification can be expressed as:

$$y = f(x) + \varepsilon \tag{1}$$

where y is the observation of the deviation from nominal value, $f(x)$ is the system error, and ε is the error term. Current profile monitoring methods have been determined the value of $f(x)$ [19,21], and some studies considered the correlations in ε [31,32]. Few researchers have addressed the problem of the correlations in. Therefore, the aim of this study is to discuss the spatial correlations of the observations and eliminate the effects of spatial correlations on circular and cylindrical profile monitoring. Based on spatial lag model (SLM) in spatial econometrics [33], considering spatial correlations among observations, this study proposes a new method for monitoring circular and cylindrical profiles in combination with control charts in SPC.

The remainder of this paper is organized as follows. In Section 2, the proposed method is introduced and an overview of this study is presented. Section 3 compares the proposed method with other methods via simulations. In Section 4, an engineering case study is presented to verify the feasibility and validity of the proposed method. Finally, Section 5 summarizes the study and explores the implications for future research.

2. Proposed method

2.1. Overview

This subsection introduces the proposed method for circular and cylindrical profile monitoring. Considering the spatial correlations of observations that often occur in the measurement points of industrial manufacturing processes, a new parametric model for the profiles is proposed. This method focuses on the geometric specifications with spatial correlations, which can be decomposed into three components: spatial correlation error, systematic error and random error. Spatial correlation error is represented by SLM model, which can express the influence of adjacent points. Systematic error comes from the regular source of error during processing. The determination of the systematic error for the circle and the cylinder will be described in detail in the subsection 2.2 and 2.3, respectively. In this method, the deviation from the nominal value of a point consists of three parts: the observations of adjacent points, the systematic error term and the error term, which can be expressed as

$$y = \sum_{s=1}^{p} \rho_s W^{(s)} y + X^{'}\beta + \varepsilon \tag{2}$$

where $X^{'} = [x_1 x_2 ... x_r]$, represents the r independent regression variables. $\beta = [b_1 b_2 ... b_r]$, represents the coefficient of r independent regression variables. $W^{(s)}$ is the s -order spatial weight matrix. The definition of $W^{(s)}$ is as follows: The weight of the adjacent s points is equal to 1 and that of the rest is equal to 0. The error term ε obeys a normal distribution with a mean of 0 and variance of σ^2. ρ is an unknown lag coefficient representing the strength of spatial correlations. The range of ρ is 0–1. When the correlation is significant, ρ is close to 1. The experimental data should be pre-treated to obtain the value of y because the circular profile should not depend on the center position and the average radius observed on each profile [23]. The value of y is calculated by subtracting the radius of the least square circle (LSC) and centered on the LSC center.

The flow diagram of this method is shown in Fig. 1 and the implementation steps are as follows:

Step 1: Establish a suitable parametric model for the profiles. In spatial correlations analysis, Moran test can be used to measure the degree of spatial correlations [35]. In the case that there are no spatial correlations, an ordinary least squares (OLS) regression model is established. In the case that spatial correlations exist, LM test is implemented to obtain more comprehensive diagnostic tests for autocorrelation. If spatial correlations of observations are more significant, a suitable model should be established based on SLM; If spatial correlations of error terms are more significant, a suitable model should be established based on spatial error model (SEM) [36,37].

Step 2: Estimate the model parameters. Based on the parametric model in step 1, the systematic error term is determined and the model parameters are estimated.

Step 3: Design charts for the parameters. According to the control chart methods in SPC, the statistics of the parameters are calculated and suitable control charts are designed to monitor the profiles.

The monitoring steps for the circular and cylindrical profiles are described in subsections 2.2 and 2.3, respectively.

2.2. Circular profile monitoring

Assume that there are M circular profiles and each circular profile $m(m = 1, 2...,M)$ has N observation points equally spaced on the circumference. The deviation of each $n(n = 1, 2, ...,N)$ point in the m th profile is represented by y_{nm}, as shown in Fig. 2. The abscissa is the value of n. Based on SLM, the circular profile model can be expressed as

$$y_{nm} = \sum_{s=1}^{p} \rho_{sm} W^{(s)} y_{nm} + X_n^{'} b_m + \varepsilon_{nm} \tag{3}$$

Due to the influence of the machine tool spindle eccentricity, vibration, ball wear and so on, the rotary parts tend to produce specific shapes during processing. Fig. 3 shows several typical features of circular profiles.

According to subsection 2.1, the monitoring steps for the circular profile are as follows:

Step 1: Establish a suitable parametric model. First, Moran test is used to measure the degree of spatial correlations. The test result is expressed in Moran index (Moran's I), which describes the degree of similarity between the observed value and the adjacent spatial elements. The Moran test is based on the least squares estimate to establish the following statistics:

$$\mathrm{I} = \frac{n}{\sum_i \sum_j W_{ij}} \times \frac{\sum_i \sum_j W_{ij}(Y_i - \bar{Y})(Y_j - \bar{Y})}{\sum_i (Y_i - \bar{Y})^2}$$

where Y_i and Y_j are observations of spatial units; $\bar{Y}$ is the average value of Y; n is the number of spatial units and W is the spatial weight matrix.

When Moran's I is greater than 0, the data presents positive correlation. The larger the value is, the greater the spatial correlation will be. When Moran's I is less than 0, the data presents spatial disparity. The smaller the value is, the greater the spatial disparity will be. Spatial data is approximately randomly distributed when Moran's I is close to zero.

Then, as introduced in subsection 2.1 step1, LM test is implemented according to the results of Moran test to obtain more comprehensive diagnostic tests for spatial correlation. The calculation process of LM test can refer to the Breusch and Pagan [37]. LM test has two statistics, LM-Lag and LM-Error, to determine whether the SLM or SEM model should be selected. If LM-Lag is more significant, a suitable model should be established based on SLM; If LM-Error is more significant, a suitable model should be established based on SEM. SLM is the mutual effect among the response variables while SEM is the influence of adjacent unit errors on the observed value.

Since the spatial correlations of observations is more significant (refer to the test results in Section 3, Table 1), the circular profile model should be based on SLM, as shown in Eq. (3).

Step 2. Determine the systematic error term

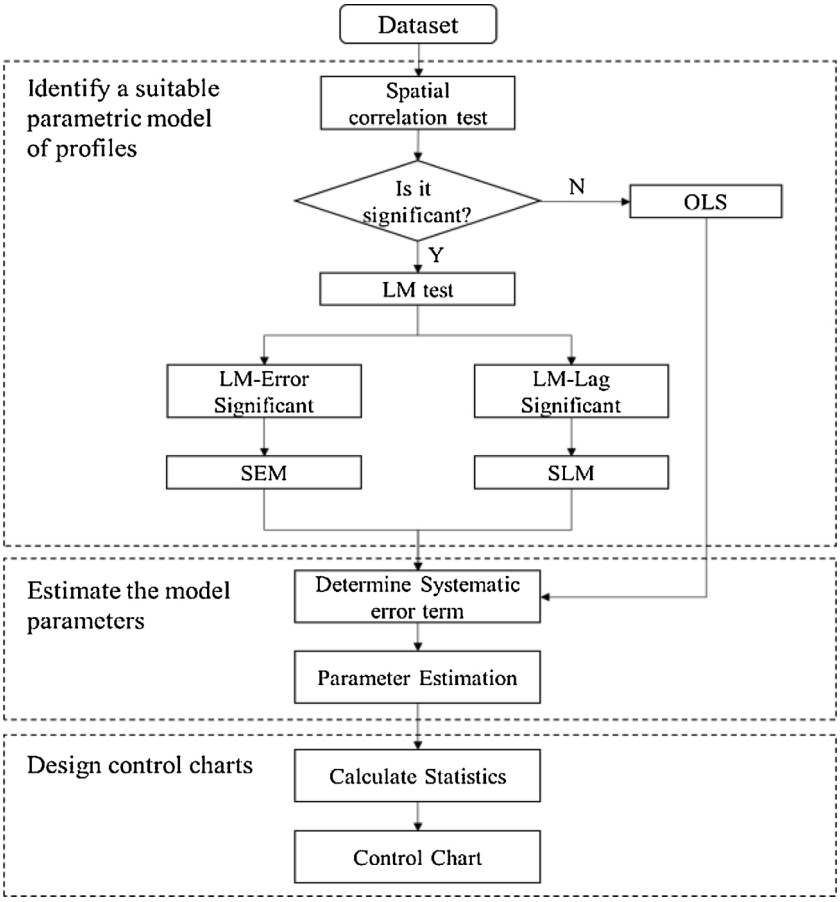

Fig. 1. Process flowchart for the proposed method.

During processing, the harmonic error that typically appears in rotary part can be regarded as a periodic function due to the rotational error of the machine tool. The research of Damir [38] indicated that the circular profile can be simulated by Fourier harmonics. They descripted the minimum number of Fourier harmonics to characterize the circular profile by the means of the frequency components decomposition. Cho & Tu [19] validated the harmonic model with a large number of actual circular and cylindrical profiles that are produced by turning and cylindrical grinding processes. Hii et al. [39] studied the relation between circular profiles and spindle motion error. A reflection mode of the spindle motion error on the circular profile was evaluated. Colosimo et al. [30] concluded the possible error forms of the spindle in the course of machining and the corresponding frequency components. Each spindle error can be characterized by specific amplitude and frequency components.

Therefore, the systematic term $X_n^{'} b_m$ in Eq. (3) can be determined by the Fourier transform given by Eq. (4). The unrelated frequency components can be filtered out or separated from the systematic term via

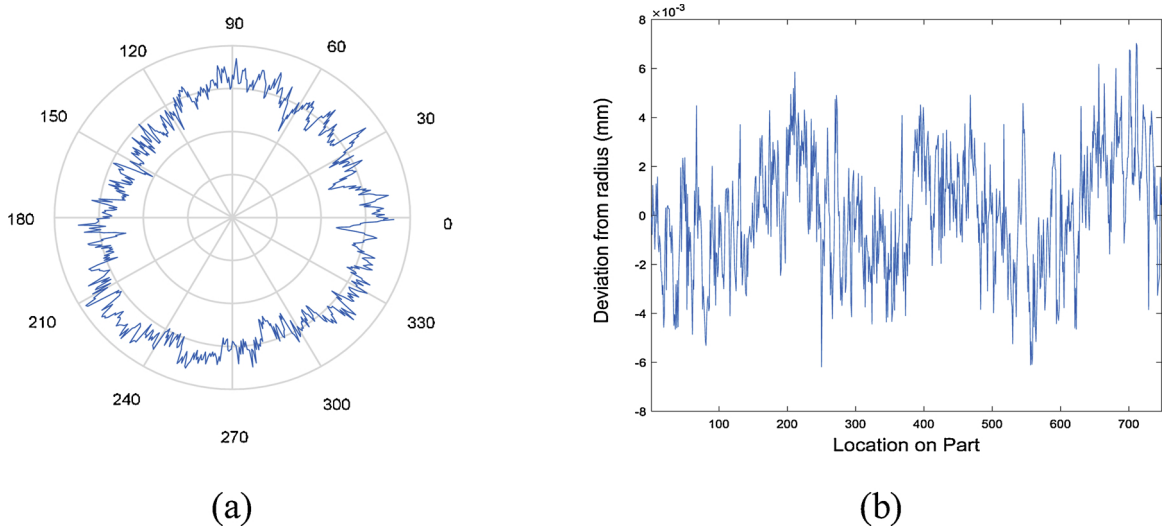

Fig. 2. (a) y_j in polar coordinate system and (b) y_j in cartesian coordinate system.

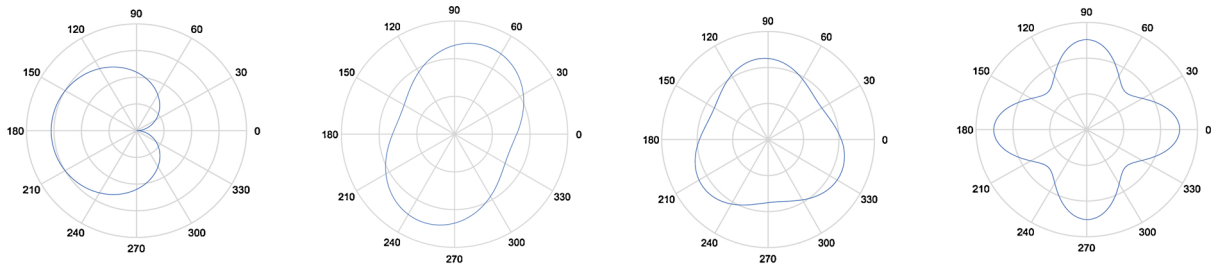

(a) Half-frequency spindle-motion error (b) Bi-lobe spindle-motion error (c) Tri-lobe spindle-motion error (d) Four-lobe spindle-motion error

Fig. 3. Circular profiles of several typical features.

the Fourier harmonic separation.

$$X_n^{'} b_m = \sqrt{\frac{1}{N}}\, b_{0m} + \sqrt{\frac{2}{N}} \sum_{k=1}^{\frac{k}{2}} [b_{2k-1m}\cos(f_k\,(t-1)) + b_{2km}\sin(f_k\,(t-1))] \tag{4}$$

where $f_k = k(2\pi/N)$; k is the k th harmonic separated by the Fourier transform; and t is the t th measurement point in the part. In order to determine the value of k, the appropriate frequency components are briefly prespecified by industrial knowledge and the frequency decompositions of experiments are also needed. In practical applications, Damir [38] have experimentally proved that the second and third harmonics are the main components in the circular frequency components. And by analyzing the weight of all amplitudes relative to the main components, they gave suggestions for the rang of the order of Fourier harmonics: 1) drilled surfaces: the 2nd harmonic to the 6th harmonic; 2) turned surfaces: the 2nd harmonic to the 10th harmonic; 3) cylindrical and centreless ground surfaces: the 2nd harmonic to the 24th harmonic.

In experiments, we can refer to the frequency components given by Damir and combine the value of frequency decomposition to determine the harmonic components.

Step 3. Parameter estimation

Parameter estimation is performed based on the determination of the systematic error term and a suitable model. The unknown parameters are ρ, β and ε. Since ε is a random error subjected to $\varepsilon \sim N(0, \sigma^2)$, the parameters that need to be estimated are ρ, β and σ^2. In the parameter estimation, it is firstly assumed that the spatial correlations can be represented by the first-order spatial weight matrix (s= 1).

The steps of parameter estimation are as follows:

Step 3.1 Estimate parameters β and σ^2 using the least-squares algorithm.

$$\hat{\beta} = (X^{'}X)^{-1}X^{'}(y - \rho Wy) \tag{5}$$

$$\hat{\sigma^2} = \frac{1}{n}(y - \rho Wy - X\beta)^{'}(y - \rho Wy - X\beta) \tag{6}$$

Step 3.2 Estimate parameter ρ using the maximum likelihood method.

The likelihood function of the model is given as

$$L(y\rho, \beta, \sigma^2) = \frac{1}{2\pi\sigma^n}\,|I_n - \rho W| \exp\{-\frac{(y - \rho Wy - X\beta)^{'}(y - \rho Wy - X\beta)}{2\sigma^2}\} \tag{7}$$

The logarithm of Eq. (7) is computed as

$$\ln L(y\rho, \beta, \sigma^2) = -ln2\pi - \frac{n}{2} ln\sigma^2 + ln\,|I_n - \rho W| - \frac{1}{2\sigma^2}(y - \rho Wy - X\beta)^{'}(y - \rho Wy - X\beta) \tag{8}$$

Input $\hat{\beta}$ and $\hat{\sigma^2}$ into Eq. (8) to obtain the following relationship

$$\ln L(y\rho) = -\frac{n}{2}(1 + ln2\pi) - \frac{n}{2}\ln(e_0 - \rho e_1)^{'}(e_0 - \rho e_1) + ln\,|I_n - \rho W| \tag{9}$$

The nonlinear optimization method is used to maximize the likelihood function and the estimated value $\hat{\rho}$ of ρ is obtained.

Step 3.3 Update $\hat{\beta}$ and $\hat{\sigma^2}$ using the new estimated value $\hat{\rho}$ in step 3.2.

Step 3.4 Repeat steps 3.1–3.3 until parameters convergence.

After obtaining the estimated values of parameters for the profile, if the residuals still have spatial correlations, the s+ 1 spatial weight matrix should be added until there are no spatial correlations in the observations.

The estimated values of the parameters can be given by

$$c_m^{'} = [\rho_m^{'}\beta_m^{'}] = [\rho_{1m}\rho_{2m}...\rho_{sm}b_{1m}b_{2m}...b_{rm}] \tag{10}$$

which have a normal distribution with mean vector μ and covariance matrix Σ.

Step 4. Design control chart

Two control charts are designed in this step: One is the T^2 control

Table 1
The geometric shape and error source of several L-F polynomial.

Fourier i	Legendre j	Fourier function F_i	Legendre polynomial P_j	Cylindrical radius feature r_{ij}	Geometric shape	Error source
0	1	0	z	z	Axial taper	misalignment of spindle/work centers
0	2	0	$(3z^2\text{-}1)/2$	$(3z^2\text{-}1)/2$	Axial bump	Workpiece deflection
1	0	cos(θ), sin(θ)	1	cos(θ) + sin(θ)	Axial eccentricity	Spindle rotation
1	1	cos(θ), sin(θ)	z	z(cos(θ) + sin(θ))	Axial tilt	Chuck clamping
1	2	cos(θ), sin(θ)	$(3z^2\text{-}1)/2$	$[(3z^2\text{-}1)/2](\cos(\theta) + \sin(\theta))$	Banana shape	Workpiece deflection and spindle rotation
2	0	cos(2θ), sin(2θ)	1	cos(2θ) + sin(2θ)	Bi-lobe circumflex	Spindle rotation

chart for the parameters, the other is the individual control chart for the residuals. Assuming the false rate is $\alpha^{'}$, the first type of error probability is $\alpha = 1 - \sqrt{1-\alpha^{'}}$.

The T^2 statistic is computed as

$$T_m^2 = (c_m - \mu)^T \Sigma^{-1} (c_m - \mu) \tag{11}$$

The upper control limit (UCL) is computed as

$$\mathrm{UCL} = \frac{(m-1)^2}{m} \beta_{\alpha, n/2, (m-n-1)/2} \tag{12}$$

When the number of parts is large ($m > 100$), $\mathrm{UCL} = \chi^2_{\alpha,n}$ can be used as an approximate control limit.

The residual statistic is given by

$$e_m = (I - \rho W) y_m - X b_m \tag{13}$$

The estimated variance of the residual is $\sigma_m^2 = \frac{e_m^{'} e_m}{n-1}$.

A traditional Shewhart-type control chart can be used to monitor σ^2. The upper and lower control limits are given as

$$\begin{aligned} \mathrm{UCL} &= \frac{\sigma^2}{n-1} \chi^2_{\frac{\alpha}{2}, n-1} \\ \mathrm{CL} &= \sigma^2 \\ \mathrm{LCL} &= \frac{\sigma^2}{n-1} \chi^2_{(1-\frac{\alpha}{2}), n-1} \end{aligned} \tag{14}$$

After obtaining the control chart limits, the quality characteristics of circular profiles can be monitored. If the statistics of the observation points are beyond the control limits, the production process is out of control and additional detection is required.

2.3. Cylindrical profile monitoring

The cylindrical profile is a three-dimensional profile consisting of multiple circular profiles. In the cylindrical coordinate system, a third coordinate for measuring the height is added to the two-dimensional polar coordinate system and represented by. In the axial direction, the measurement points are equally spaced and points with the same z value constitute a layer; each layer is regarded as a circular profile. In the radial direction, the position of a point is represented by θ. Therefore, the radius of a measurement point on the cylindrical coordinate system can be obtained by z and θ, and is expressed as $r(z, \theta)$.

Unlike in the circular profile, radial and axial errors both exist in the cylindrical profile. The radial error is represented by the Fourier series as the circular profile. In the axial direction, the misalignment of spindles and work centers, workpiece deflection, and thermal expansion etc. will cause axial errors [40]. Zhang et al. [21] analyzed the effects of various error sources on the geometric error of cylindrical parts and showed that the axial errors which are created in cylindrical workpieces by manufacturing error sources can be modelled by the Legendre polynomial. The Legendre polynomial is complete and orthogonal, which ensures the independence of the coefficients. Therefore, the Legendre polynomial is basically consistent with the axial direction error of the cylindrical characteristics, the axial error can be represented by the Legendre polynomial as in Eq. (15).

$$\begin{aligned} P_0(z) &= 1 \\ P_1(z) &= z \\ P_2(z) &= \frac{1}{2}(3z^2 - 1) \\ P_3(z) &= \frac{1}{2}(5z^3 - 3z) \\ P_4(z) &= \frac{1}{8}(35z^4 - 30z^2 + 3) \end{aligned} \tag{15}$$

By analyzing the combination of Legendre polynomial and Fourier function, we can get cylindrical profiles of different shapes. Glenn [41] used the multiplication of the axial and radial functions to represent the radius errors. Zhang et al. [21] analyzed the possible forms of axial errors. They confirmed that the form error can be expressed by the polynomial of z. And they also utilized the Legendre-Fourier (L-F) polynomial to express the systematic error term of the cylindrical profile. The L-F polynomial is the multiplication of the Fourier and Legendre function and can be used to model the cylindrical error, which is presented in Equation (16).

$$\begin{aligned} r(z, \theta) &= r_0 + \Delta r(z, \theta) \\ &= \sum A_{0j} P_j(z) + \sum \sum [A_{ij} P_j(z) \cos(i\theta) + B_{ij} P_j(z) \sin(i\theta)] \end{aligned} \tag{16}$$

where $z \in [-1,1]$; $\theta \in [-\pi, \pi]$; $P_j(z)$ is the j th Legendre polynomial function indicating the deviation in the z-axis direction; $\cos(i\theta)$ represents the deviation in the x-axis direction and $\sin(i\theta)$ represents the deviation in the y-axis direction. $\cos(i\theta)$ and $\sin(i\theta)$ make up the radial variation of the cylinder, which can be represented by F_i. r_0 is the average radius of the workpiece and can be calculated as $\sum A_{0j} P_j(z)$. Δr is the shape error at the (z, θ) point and can be calculated by the multiplication of the Fourier and Legendre functions. The coefficients in the L–F polynomial can be calculated as

$$A_{ij} = \frac{\sum_{k=1}^{t} \sum_{l=1}^{u} r_{kl} P_j(z_k) \cos(i\theta_l)}{\sum_{k=1}^{t} \sum_{l=1}^{u} P_j^2(z_k) \cos^2(i\theta_l)} \tag{17}$$

$$B_{ij} = \frac{\sum_{k=1}^{t} \sum_{l=1}^{u} r_{kl} P_j(z_k) \sin(i\theta_l)}{\sum_{k=1}^{t} \sum_{l=1}^{u} P_j^2(z_k) \sin^2(i\theta_l)} \tag{18}$$

where k is the order of a point in z axis; t is the total number of points in z axis; l is the order of radial azimuth and u is the total number of radial azimuths. The value of A_{0j} can also be estimated by Eq. (17).

Table 1 and Fig. 4 shows several typical features of cylindrical profiles, where $P_j F_i$ represents the order of the L-F polynomial.

Similar to the monitoring process for circular profiles described in subsection 2.2, the steps of the cylindrical profile monitoring can be defined as follows:

Step 1. Same as the circular space correlations test in subsection 2.2, step 1. Moran and LM test are performed to test cylindrical spatial correlations and to choose an appropriate model.

Step 2. Determine the systematic error term. Because the average radius has been removed from the observed value. The first part on the right of Equation (16) should be ignored in the systematic error term. Therefore, the systematic error term can be written as

$$X_n^{'} b_m = \sum \sum [A_{ij} P_j(z) \cos(i\theta) + B_{ij} P_j(z) \sin(i\theta)] \tag{19}$$

The values of i and j corresponding to the order of Fourier function and Legendre polynomial can be briefly prespecified by industrial knowledge and also be determined by the frequency decomposition of measurements. Damir [38] proposed the significant harmonics of cylindrical surfaces for reference, but they did not give the value of the corresponding polynomials. Colosimo et al. [28] gave six basic components that were shown to be significant to describe the cylindrical surfaces. We also utilize these six orders of polynomials as the basic components to represent the cylindrical profile errors in experiments. The corresponding polynomial is shown in Table 2.

Step 3. Estimate the parameters of the selected model. Because the cylinder is spatial, the value of the weight matrix is different from that in the circular profile. After aligning the cylindrical measurements, the weight matrix can be represented by the rook-based contiguity (points adjacent to a certain point in four directions, weighted to 1) or the queen-based contiguity (points adjacent to a certain point in eight directions, weighted to 1).

Step 4. The design process for the cylindrical profile control charts is the same as that in the circular profile monitoring, as described in subsection 2.2. T^2 and the residual statistics are calculated using Eqs. (11) and (13) and the control limits are obtained using Eqs. (12) and (14).

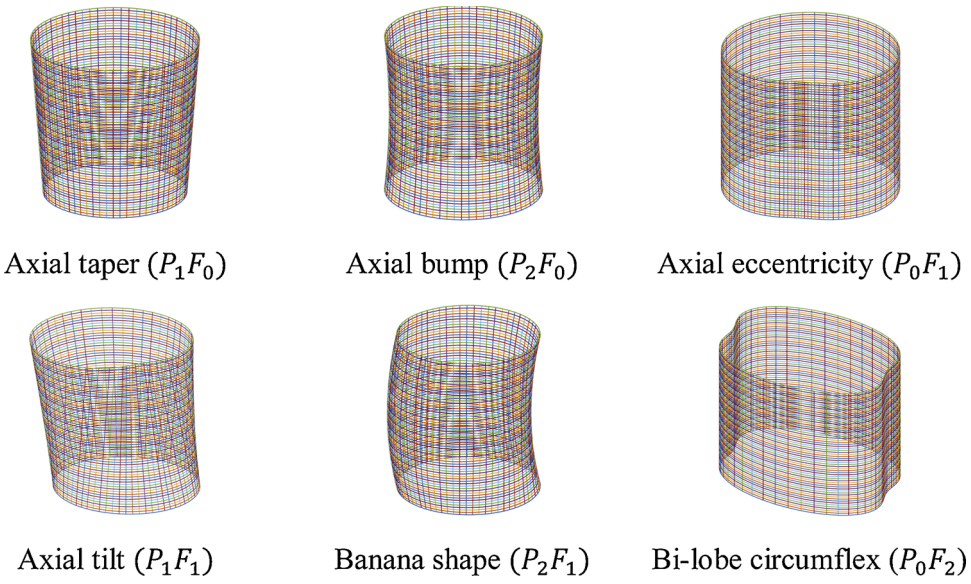

Fig. 4. Cylindrical profiles of several typical features.

Table 2
The basic components of L-F polynomial.

k	Order of Legendre polynomial	Order of Fourier function	L-F
1	0	2	cos2 θ+ sin2θ
2	0	3	cos3 θ+ sin3θ
3	1	0	z
4	1	2	z(cos2 θ+ sin2θ)
5	1	3	z(cos3 θ+ sin3θ)
6	2	0	$(3z^2\text{-}1)/2$

3. Simulation

3.1. Circular profile

The experimental parts presented by Colosimo et al. [30] are used as references in this subsection. The authors sampled 100 C20 cylinders machined from an original diameter of 30 mm to a nominal diameter of 26 mm as experimental parts. A total of 748 points were sampled in each circular profile by using a coordinate measuring machine (CMM).

3.1.1. Simulation experiment

The simulation data is processed based on the circular profile monitoring process described in subsection 2.2. The steps are as follows:

Step 1. Establish a suitable parametric model.

First, the spatial correlation of each profile is examined by the Moran and LM test. In the actual operation, Matlab space measurement toolbox 'jplv7' can be used in the Moran and LM test. The test results are presented in Table 3. As can be seen from the results in the table, there is strong spatial correlations among the observations according to the result of Moran test. And according to the results of LM test, the LM-Lag is more significant, which proves that there are strong correlations in observations. Therefore, it is reasonable to establish a SLM-based model.

Table 3
Results of Moran and LM test.

Statistics	Statistical value	P value
Moran-istat	19.0004	0.000
LM (lag)	139.3217	0.000
LM (error)	13.5151	0.000

Step 2. Determine the systematic error term

In this step, the decomposition is implemented by harmonic separation. The first Fourier harmonic $b_{0m}(k = 0)$ reflects the position of the center of the circle and the second Fourier harmonic $b_{1m}(k = 1)$ is the nominal radius of the sampled profiles. Since the circle in the experiment has its center at the origin and the nominal radius is subtracted from the observations, the values of b_{0m} and b_{1m} are both zero. The value of k is obtained by the Fourier decomposition. Taking the former 50 harmonics, as shown in Fig. 5, the Fourier decomposition exhibits strong amplitudes in the 2nd and 3rd harmonics while others are almost zero and can be ignored. therefore, the systematic error term in this case is represented by k = 2, 3 harmonics, and written as

$$X_n^{'} b_m = \sqrt{2/N}\,[b_{3\mathrm{m}}\cos(f_2(t-1)) + b_{4\mathrm{m}}\sin(f_2(t-1)) + b_{5\mathrm{m}}\cos(f_3(t-1)) + b_{6\mathrm{m}}\sin(3(t-1))] \quad (20)$$

Step 3. Parameter estimation

First, the first-order correlation matrix is selected to estimate the parameters. ρ and β are calculated as in subsection 2.2 and expressed as $c_m^{'} = [\rho_m^{'}\beta_m^{'}] = [\rho_m b_{1m} b_{2m} b_{3m} b_{4m}]$. Next, the Moran test is used to analyze the spatial correlations of the residuals until the results of the test statistics are not significant.

Step 4. Design control chart

The T^2 statistics of these 100 profiles are calculated according to Eq.

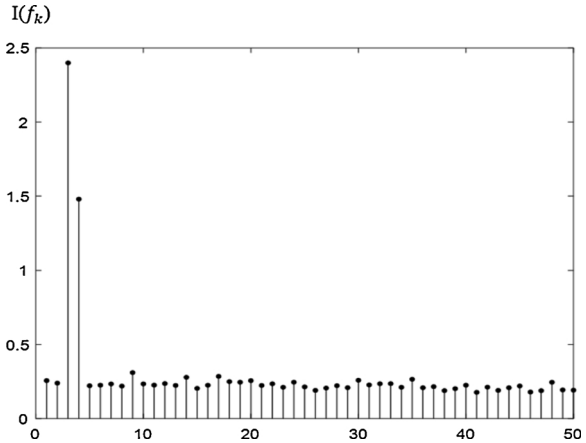

Fig. 5. Fourier decomposition map for the former 50 harmonics of simulated circular profiles.

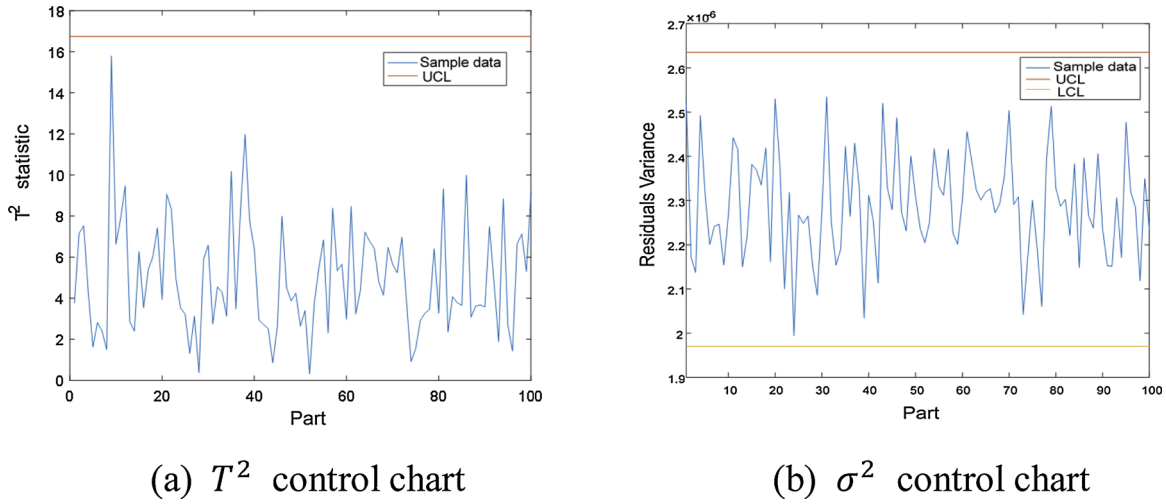

(a) T^2 control chart (b) σ^2 control chart

Fig. 6. Control charts of 100 circular profiles in phase I.

(11). Assuming the false rate $\alpha^{'} = 1\%$ for each control chart, the probability of type I error is $\alpha = 1 - \sqrt{1-\alpha^{'}} = 0.5013\%$. The upper control limit is UCL= $\chi^2_{0.005013,5} = 16.7496$. The control limits of σ^2 are calculated by Eqs. (13) and (14). Fig. 6 shows the T^2 and σ^2 control charts for the 100 simulated circular profiles in phase I.

3.1.2. Method comparison

The comparison of the proposed method with other methods, based on the dataset provided by Colosimo et al. [30], is described in this subsection. Currently, there exist several common methods for monitoring circular profiles.

1 Out-of-roundness (OOR)
OOR is the degree of the cross-section close to the theoretical circle, which is used to evaluate the accuracy of circularity. The LSC method is a common and convenient method to calculate the OOR value; the OOR value is calculated using the difference between the maximum and the minimum distance from the actual profile to the least squares circle. Each circular profile corresponding to an OOR value can be monitored using the Shewhart control chart. If the corresponding OOR value is not larger than the upper control limit, the circular feature conforms to the requirement.

2 Location Control Chart (LOC)
LOC is proposed by Boeing Commercial Airplane Group [[34]]. This method collects measurement data at each location and monitors the measurements by plotting them in the same coordinate system. After profiles registration (the process of feature registration algorithm can be referred to Colosimo and Pacella [23]), the Shewhart control chart is applied to each observation point under controlled conditions. If the observed shape is in control, the observations should be within the control limits with a given probability. The control limits of the LOC are calculated by the mean and standard deviation of these measurement points on the same position.

3 Spatial Autoregressive Regression (SARX)
SARX is proposed by Colosimo et al. [30] to monitor circular profiles. This method is based on the SEM which considers the effect of spatial correlations on residuals. They assumed that the observations on each profile is consist of systematic term and error term. Comparing with Eq. (2), the expression of observations based on SEM can be written as follows:

$$y = X^{'}\beta + v$$

$$v = \lambda W v + \varepsilon$$

where $X^{'}\beta$ is the systematic term; v is the error term; W is the weight matrix and λ is the coefficient of spatial correlations. Based on the regression method, the author proposed a residual correlation model used in combination with control charts. This method considers the effect of spatial correlations on residuals and analyzes the monitoring process of circular profiles. The difference between SLM model and SARX model is the representation of spatial correlations. In SLM, spatial correlations are represented in a separate term. While in SARX, spatial correlations are included in the error term. These two methods are based on the different models and have different effects. For better comparison, T^2 and residuals control charts are both used in these methods. The difference is the value of the statistics and the control limits.

4 Principal Component Analysis (PCA)
PCA is also a practicable method in circular profile monitoring. Colosimo and Pacella [23] used PCA to identify systematic patterns in roundness profiles. Wang et al. [25] used this method to monitor the multimode near-circular shape profiles. In this paper, PCA is used as a comparison method by the means of monitoring the T^2

Table 4
Mean of ARL results for 1000 simulations in phase II.

	δ	OOR	LOC	SARX	PCA	SLM-based
Spindle	$\delta_1 = 0.005$	49.41	63.33	23.48	66.67	**23.17**
	$\delta_1 = 0.01$	54.23	60.44	13.88	18.18	**12.2**
	$\delta_1 = 0.05$	53.96	4.63	**1.37**	5.71	1.53
	$\delta_1 = 0.1$	78.48	1.02	1.23	2.06	**1**
Bi-lobe	$\delta_2 = 0.005$	66.83	10.54	4.86	76.92	**4.3**
	$\delta_2 = 0.01$	18.42	**1.06**	1.28	19.23	1.2
	$\delta_2 = 0.05$	1	1	1	1.78	1
	$\delta_2 = 0.1$	1	1	1	1	1
Tri-lobe	$\delta_3 = 0.005$	61.53	10.58	5.14	52.63	**4.95**
	$\delta_3 = 0.01$	10.77	**1.05**	1.23	7.69	1.32
	$\delta_3 = 0.05$	1	1	1	1.38	1
	$\delta_3 = 0.1$	1	1	1	1	1

Table 5
Polynomial orders in the simulation.

Order of Legendre polynomial	Order of Fourier component	x_{kn}
0	0	$P_0(z)$
1	2	$P_1(z)\cos(2\theta)$
1	2	$P_1(z)\sin(2\theta)$
2	0	$P_2(z)$

Table 6
Mean of ARL results in phase II.

	δ	OOR	LOC	SARX	PCA	SLM-based
Axial error	$\delta_1 = 0.01$	50.47	39.29	20.51	77.78	**15.1**
	$\delta_1 = 0.05$	43.15	24.67	1.83	46.67	**1.61**
	$\delta_1 = 0.1$	27.51	5.82	**1.32**	27.77	1.35
Radial error	$\delta_2 = 0.01$	54.73	31.94	5.62	83.34	**5.38**
	$\delta_2 = 0.05$	48.69	**1.63**	2.83	28.57	2.64
	$\delta_2 = 0.1$	10.93	**1**	2.64	1.60	2.76
Both	$\delta_3 = 0.01$	63.14	36.23	19.07	66.67	**18.28**
	$\delta_3 = 0.05$	68.59	15.87	1.63	39.16	**1.59**
	$\delta_3 = 0.1$	46.16	2.91	**1.13**	18.18	1.21

statistics of principal components and the squared prediction error (SPE). We retain the principal components which can explain over 80 % of the total variance.

This subsection describes the comparison of the performances of these methods in phase II. The goal of phase II is to detect changes in the monitoring process as promptly as possible. The monitoring approaches are compared in terms of the average run length (ARL), which is defined as the number of parts tested until the first out-of-control signal is recorded. Therefore, assuming that the false-alarm probabilities of these methods are equal to 1 % in phase I, 1000 circular profiles with the same parameter distribution are simulated to obtain the control limits of these methods. To evaluate the performance in phase II, simulations are performed under a total of three out-of-control conditions: spindle motion error, bi-lobe error and tri-lobe error.

1) Spindle motion error: $y_n(p) + \sqrt{\frac{2}{p}}\delta_1 \sin(\frac{1}{2}\theta_p)$;

2) Bi-lobe error: $y_n(p) + \sqrt{\frac{2}{p}}\delta_2[c_{1n}\cos(2\theta_p) + c_{2n}\sin(2\theta_p)]$;

3) Tri-lobe error: $y_n(p) + \sqrt{\frac{2}{p}}\delta_3[c_{3n}\cos(3\theta_p) + c_{4n}\sin(3\theta_p)]$.

In phase II, each condition is simulated 1000 times to obtain the average of ARL. The ARL results of these methods under the three conditions are presented in Table 4. Performance comparison is obtained by simulating profiles according to the phase II models previously described and computing the ARL obtained by using the control limits in the phase I.

Table 4 shows that the proposed method has the lowest ARL value in most cases. LOC and SARX also perform well in bi-lobe and tri-lobe cases. When δ is small, which means that the change is not obvious, the SLM-based and SARX methods have good performance compared with the other methods. The LOC method demonstrates acceptable performance as well when the change is obvious. The OOR method is least effective because the OOR value cannot reflect the original shape of the profile. The effect of PCA is not as good as expected. It is not sensitive to minor changes. As can be seen from the results in Table 4, the methods of considering spatial correlations are obviously better than the ordinary method.

3.2. Cylindrical profile

3.2.1. Simulation experiment

In this stage, 100 cylinders are simulated using the parameters listed in Table 5. In each cylindrical profile, 10 layers are sampled with 98 points per layer.

Similar to the procedure of circular profile monitoring, first, the Moran and LM tests are performed for the observations to establish a suitable spatial correlation model. Next, the parameters and T^2 statistics are calculated. Last, two control charts for monitoring the T^2 statistics and residuals are designed to obtain the monitoring results. The simulation results are presented in the next subsection.

3.2.2. Method comparison

On referring to the case of the circular profiles, the five methods: OOR, LOC, SARX, PCA and SLM-based can be implemented to monitor the cylindrical profiles. In phase I, 1000 cylindrical profiles are simulated to calculate the control limits of these methods with the false-alarm probability equal to 1 %. Therefore, the control limits can be used as references in phase II. To evaluate the performance in phase II, simulations are performed by adding axial and radial errors, represented by the following models:

1) Axial error: $\delta_1 P_2(\cos(2\theta) + \sin(2\theta))$;

2) Radial error: $\delta_2 P_0(\cos(4\theta) + \sin(4\theta))$;

3) Axial and radial errors: $\delta_3 P_2(\cos(4\theta) + \sin(4\theta))$.

In this simulation, each condition is simulated 1000 times to obtain the average of ARL in phase II. The mean of the ARL of these methods is given in Table 6.

Table 6 shows that SLM-based and SARX methods are significantly superior to others. In the case of obvious changes, the results of LOC are close to those of the SLM-based and SARX, and they all demonstrate satisfactory results in comparison with those of OOR and PCA methods. The PCA is not sensitive in the small change situations and the OOR method is the least effective method of the five methods. In general, the SLM-based method obtains the lowest ARL value in most cases. It can also be seen from Table 6 that the axial error is easier to detect than the radial error.

4. Case study

This section describes the validation of the performance of the proposed method using the cylinder bores of B12 serial engines (Fig. 7(a)). The cylindrical features of engine cylinder bore are typically generated by honing operations. The experimental setup is shown in Fig. 7(b). The cylindrical hole is machined by the vertical and rotational motion of the honing head. The standard diameter of the bore is 71 mm and the actual diameters are measured using a coordinate measuring machine. Twelve engines (including six qualified engines and six unqualified engines which were honed to destroy the shape of the cylinder) including 48 bores are chosen as the experimental objects. Ten

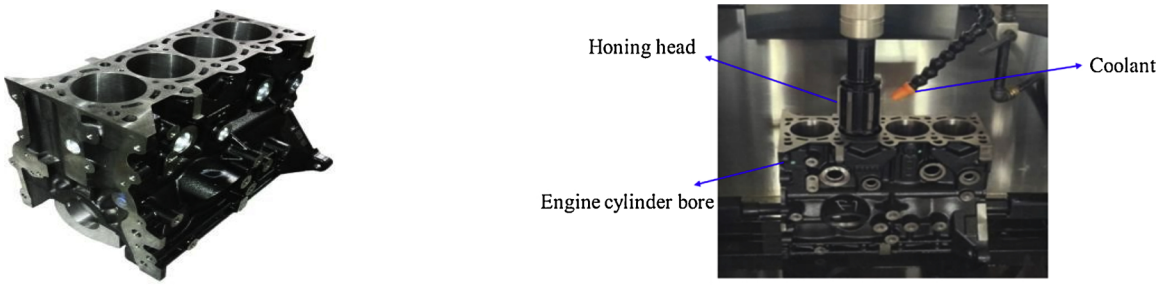

(a) B12 engine with four-cylinder bores. (b) Bore honing experimental system.

Fig. 7. (a) B12 engine with four-cylinder bores. (b) Bore honing experimental system.

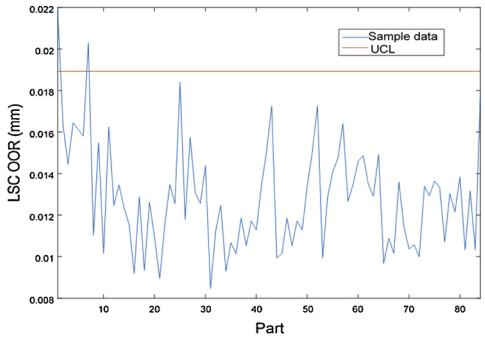

(a) Control chart of OOR method.

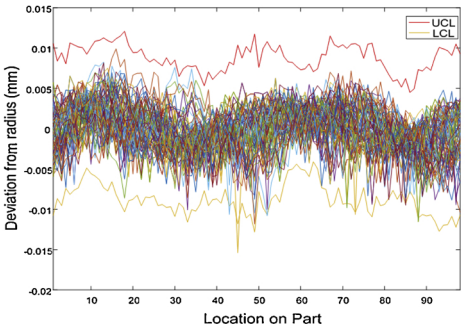

(b) Control chart of LOC method.

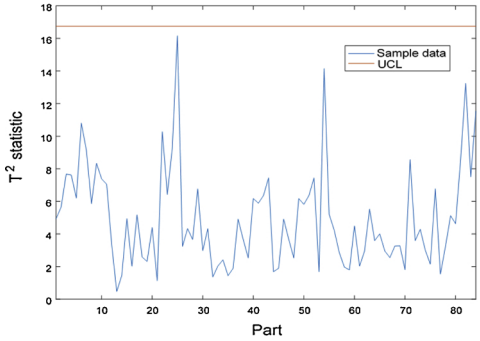

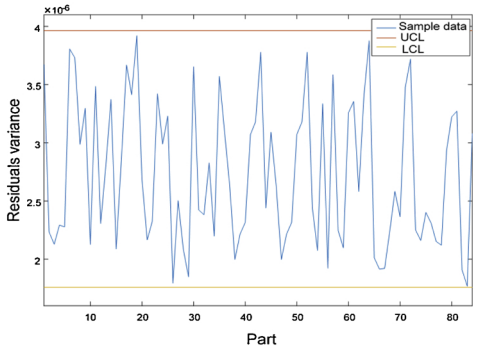

(c) T^2 and residual control charts for the SARX method.

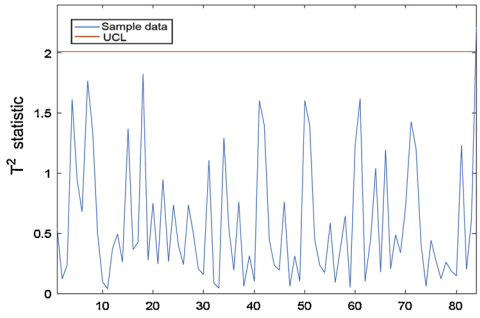

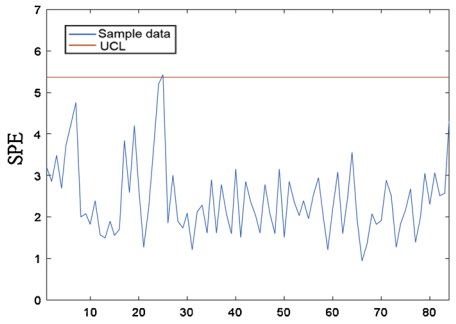

(d) T^2 and residual control charts for the PCA method.

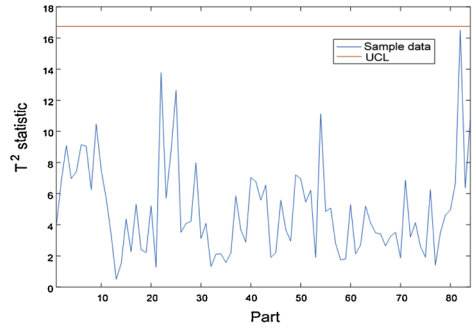

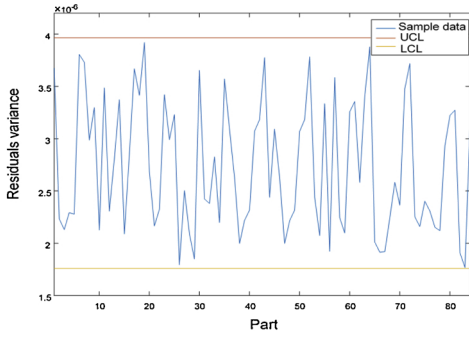

(e) T^2 and residuals control charts for the SEM-based method.

Fig. 8. Circular profile control charts for the five methods in phase I.

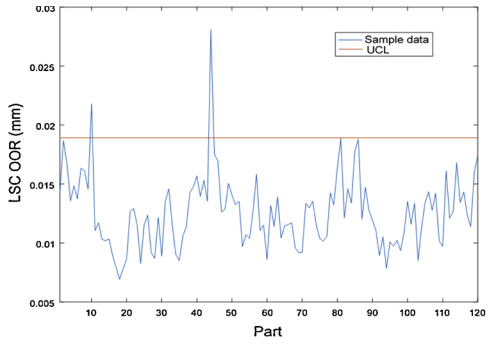

(a) Control chart of OOR method.

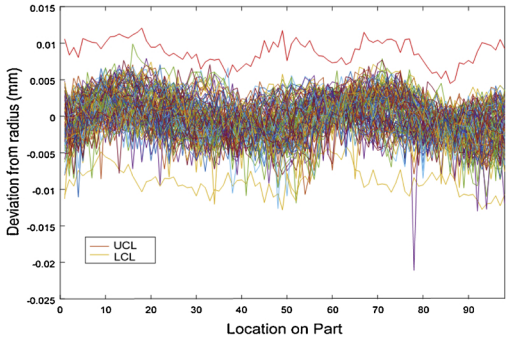

(b) Control chart of LOC method.

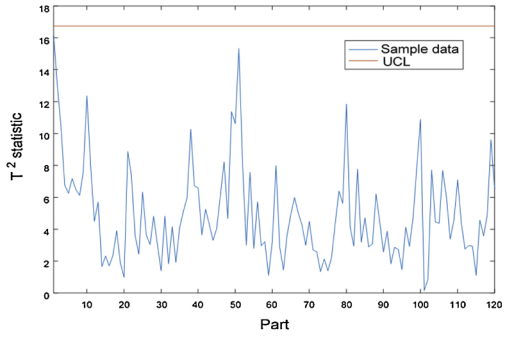

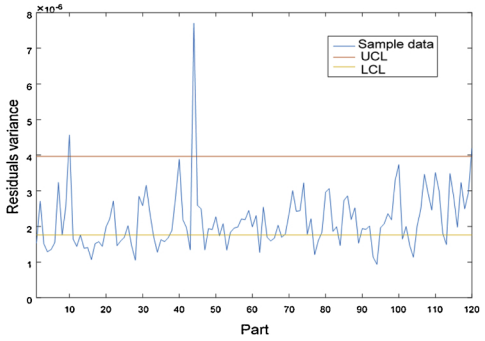

(c) T^2 and residual control charts for the SARX method.

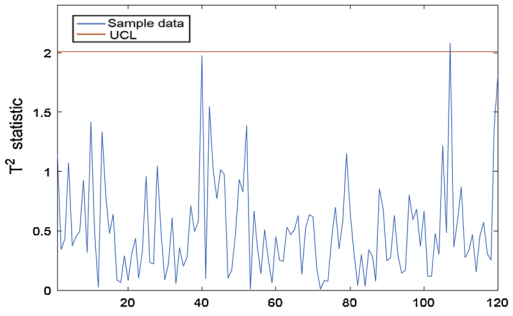

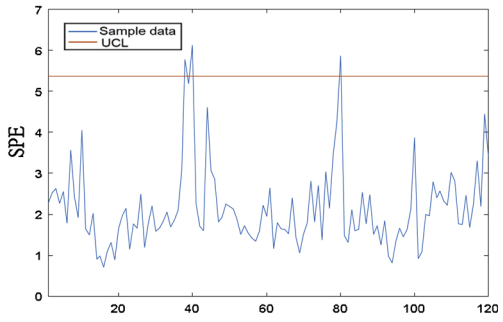

(d) T^2 and residual control charts for the PCA method.

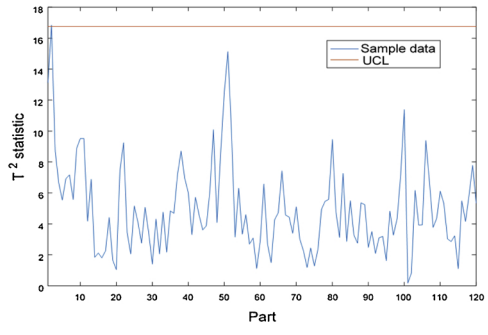

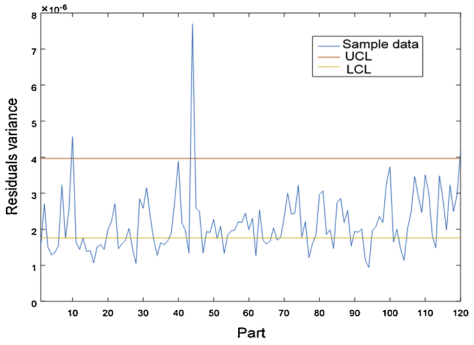

(e) T^2 and residuals control charts for the SEM-based method.

Fig. 9. Circular profile control charts for the five methods in phase II.

Table 7
Number (rate) of unqualified parts detected using the five methods.

Number of unqualified parts	OOR 2	LOC 30	SARX 45	PCA 4	SLM-based 47
detected	1.67 %	25 %	37.5 %	3.33 %	39.2 %

layers in each bore with 98 points per layer are sampled using the CMM.

4.1. Circular profile

Eighty-four qualified circles are chosen as phase I objects and the control limits are obtained from them. OOR, LOC, SARX, PCA and SLM-based methods are implemented in these 84 circular profiles in phase I. The results are shown in Fig. 8.

In phase I, the historical samples are analyzed to identify the in-control process behavior. The control limits of each method are obtained through the calculations. There are eleven shapes out of control when using the LOC method, while the Type I error rates of the other methods are within acceptable limits. Therefore, the LOC method is too strict in phase I and it is not suitable for use in this case.

In phase II, the number of out-of-control parts detected by these methods is compared. One-hundred-and-twenty circular profiles from unqualified engine bores are selected to compare the detection rates of the considered methods. Fig. 9 shows the OOR, LOC, SARX and SLM-based control charts of the 120 circular profiles in phase II. Table 7 lists the number of unqualified parts detected using these methods.

Fig. 9 and Table 7 show that the detection results of SARX and SLM-based methods are notably higher than those of the OOR, PCA and LOC methods. Combining with Fig. 8, the false-alarm probability of LOC is extremely high in phase I, and thus, it is not suitable for use in this case. SARX and SLM-based methods exhibit similar results because they both consider the impact of spatial correlations. The OOR and PCA method can barely detect the out-of-control situation in this case.

In this case, the detection rate of SLM-based method has a significantly improvement compared with OOR and PCA methods. Furthermore, the SLM-based method demonstrates better results than the SARX method does, which verifies the spatial correlation test results that the spatial correlation in observations is more significant. But overall, the detection rates of these methods are very low, so that the unqualified parts are difficult to detect. The cause of this phenomenon may be the selected samples are unqualified cylinders, for which the circularities are under control.

4.2. Cylindrical profile

Similar to the circular profile monitoring, five methods: OOR, LOC, SARX, PCA and SLM-based are used to monitor the cylindrical profiles. Forty-eight cylinders are evaluated to compare the performance of these methods. Fig. 10 shows the radial errors of 24 qualified and 24 unqualified cylinder bores.

With reference to the in-control machined surfaces, control charting aims at detecting the possible out-of-control shapes in this set of items. To obtain the control limits of the control charts in phase I, the control charts pertaining to the five methods are shown in Fig. 11.

In Phase I, the control limits can be obtained from the in-control cylindrical profiles and act as a reference for phase II. Meanwhile, the control charts show that the sample profiles are within the control limits except for the 16th part considered in the SARX method and the 17th part considered in the SPE control chart of PCA. Due to the small sample size in this experiment, the false rate of these two methods is 4.17 % and cannot be neglected. But these methods are still used as comparison methods in phase II.

In phase II, the performances of these methods are evaluated via the detection rate. The number of out-of-control parts detected by these methods are compared. Fig. 12 shows the control charts of 24 out-of-control cylindrical profiles in phase II; Table 8 presents the number of unqualified parts detected by these methods.

As can be seen from the Fig. 12 and Table 8, the detection rate of the SLM-based method is the highest and the second highest rate is that of the SARX method, approximately the same as that of the SLM-based method. The OOR method is the least effective. The PCA test results are the same as LOC but there is a point beyond the control limit in phase I.

In the case of cylindrical profiles, the SLM-based method demonstrates better performance than SARX does and the detection rate has been improved 8.3 %, which indicating that the spatial correlations in observations are more in line with the actual situation.

The difference between SARX and SLM-based method is based mainly on the T^2 statistics and the value of residuals, because both the SARX and SLM-based method eliminate the influence of spatial correlations. T^2 control chart is monitoring the coefficients of spatial correlations and the systematic error. Since the two methods have different representations of spatial correlations, the corresponding T^2 statistics are different. In Fig. 12, phase II, The T^2 control chart of SLM can detect two additional out-of-control parts: the third point and the twenty-third point. The other advantage of SLM-based method is that in the T^2 control chart of phase I, Fig. 11, the 16th T^2 statistic of SARX is obviously out of the control limits, which will cause erroneous judgment that the controlled part will be recognized to be out of control.

Moreover, the detection rate for cylindrical profiles is notably higher than that for circular profiles. One of the possible reasons is that the axial change of a cylinder is easier to detect than the radial change; another is that the selected samples are unqualified cylinders, for which the circularities are under control.

4.3. Error form analysis

Error form analysis can help engineers examine the cause of the errors for the machined parts and improve the processing technology. By removing the effects of random errors and analyzing the systematic

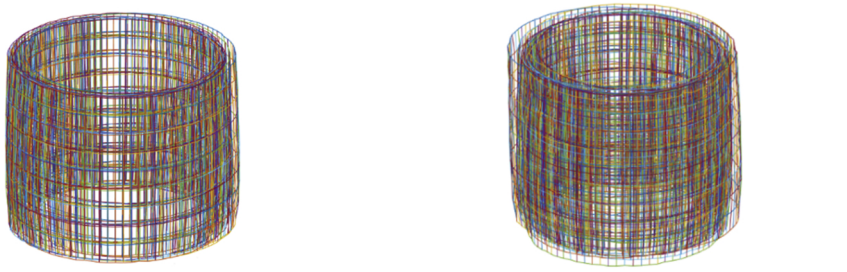

(a) 24 qualified cylinder profiles. (b) 24 unqualified cylinder profiles.

Fig. 10. Radial errors of cylindrical profiles.

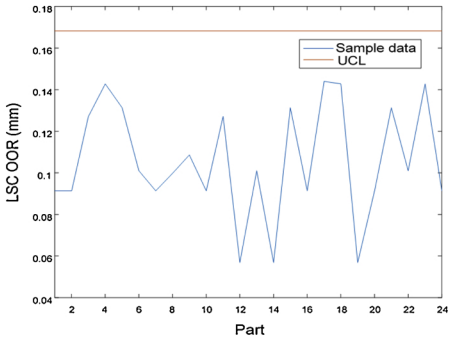

(a) Control charts of OOR method

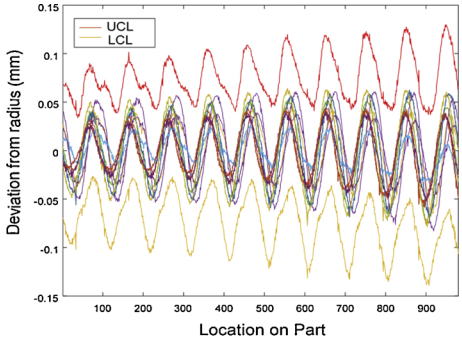

(b) Control charts of LOC method

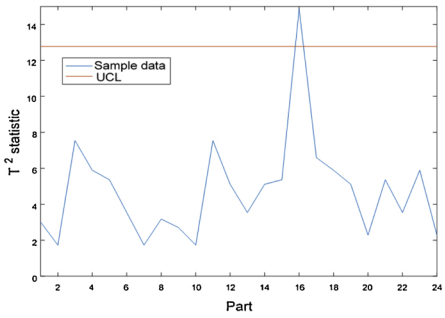

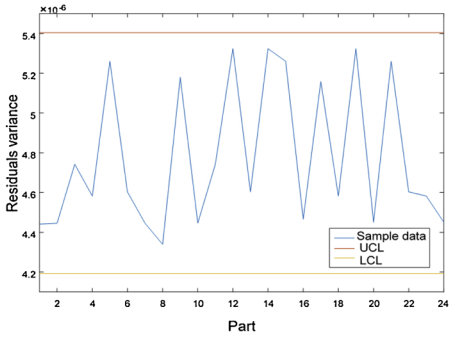

(c) T^2 and residual control charts for the SARX method

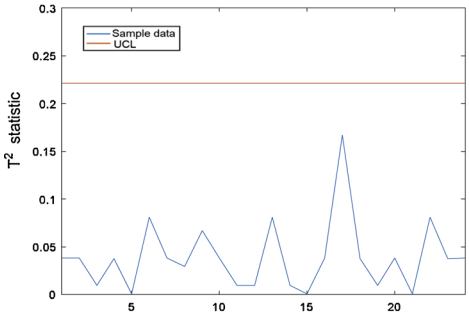

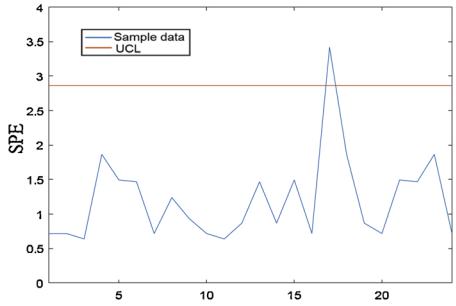

(d) T^2 and residual control charts for the PCA method

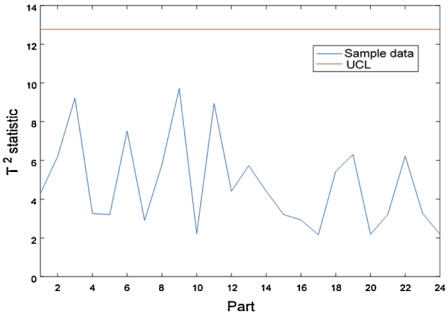

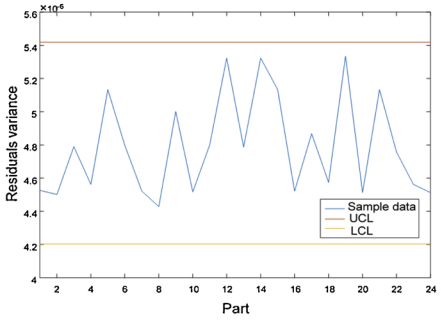

(e) T^2 and residual control charts for the SLM-based method

Fig. 11. Cylindrical profile control charts for the five methods in phase I.

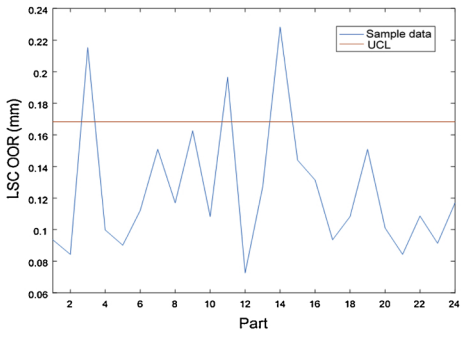

(a) Control charts of OOR method

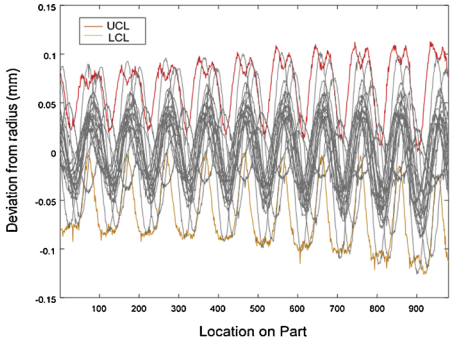

(b) Control charts of LOC method

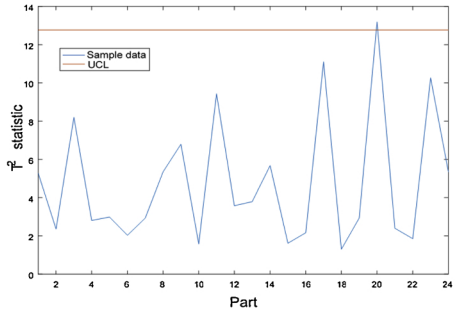

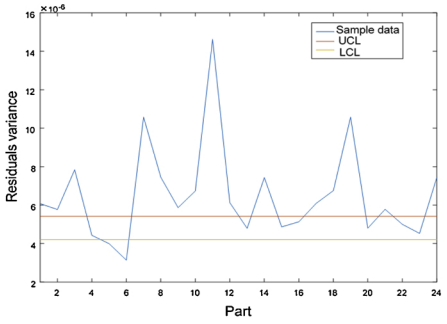

(c) T^2 and residual control charts for the SARX method

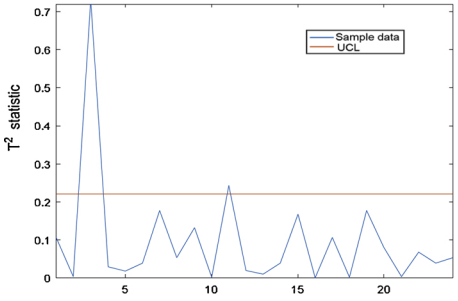

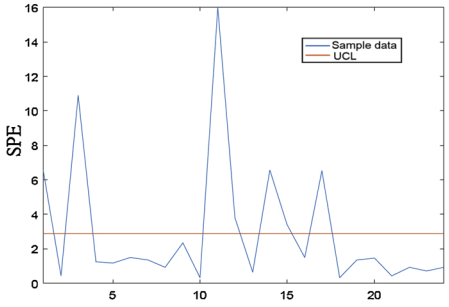

(d) T^2 and residual control charts for the PCA method

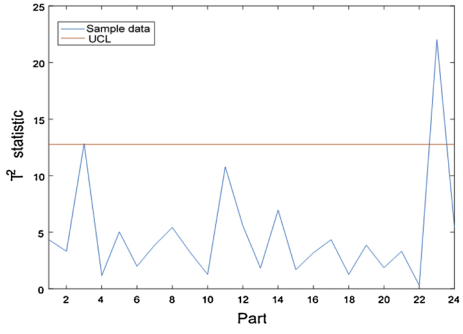

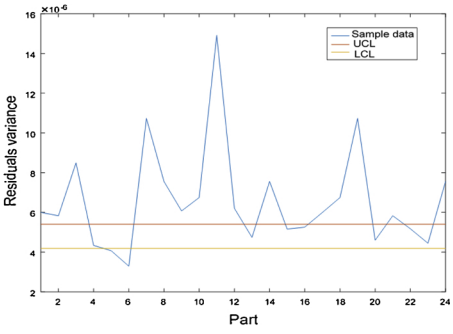

(e) T^2 and residual control charts for the SLM-based method

Fig. 12. Cylindrical profile control charts for the five methods in phase II.

Table 8
Number (rate) of unqualified parts detected using the five methods.

Number of unqualified parts	OOR 3	LOC 7	SARX 18	PCA 7	SLM-based 20
detected	12.5 %	29.2 %	75%	29.2 %	83.3 %

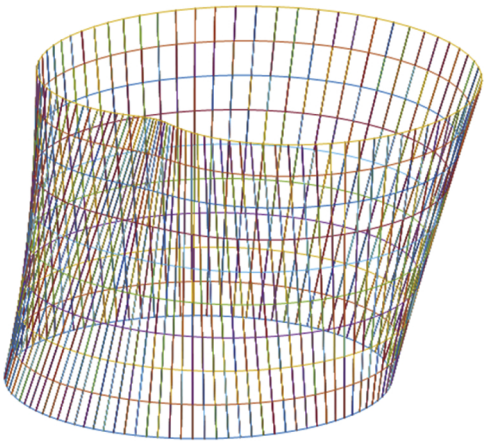

Fig. 13. Schematic of unqualified cylinders.

errors of out-of-control parts, the cause of the error can be obtained and corrected during the manufacturing process. In this case, the schematic of the corresponding error form is shown in Fig. 13. As seen, the error appears as a radial half-frequency and axial tilt. According to the analysis of machining errors of cylindrical parts carried out by Zhang et al. [21], the possible reason for the radial half-frequency error is whirling or the presence of a ball bearing with a worn ball, and axial tilt errors can occur due to the misalignment of spindle or work centers. Based on the results of the analysis, the possible reasons of the machined error can be determined, and the processing stage can be improved in a targeted manner.

5. Conclusion

Geometric profile monitoring has traditionally faced the problem pertaining to measurement points with spatial correlations. There exist methods such as OOR, LOC, PCA and SARX. The former three do not consider the spatial correlations, while the SARX method takes into account the spatial correlations in the error term. This paper discusses the spatial correlations of observations and proposes a SLM-based method for circular and cylindrical profile monitoring. Taking engine cylinder bores as an example, the detection rates of the proposed method demonstrate an improvement of 1.7 % and 8 % in the circular and cylindrical profiles compared with SARX. Besides, these results are much better than those obtained by the other methods. In addition, the PCA method is not effective in this case and another disadvantage of PCA is that the principal components may be a combination of multiple error shapes and difficult or impossible to interpret. Although both SLM-based and SARX models consider spatial correlations, these two models represent different spatial interaction effects. SLM is the mutual effect among the response variables; SARX is the influence of the adjacent units' errors on the observed value. In the case study, the results of phase II indicated that the performance of considering spatial correlations methods is better than the performance of the ordinary methods, and the results also indicated that the spatial correlations in observations are more in line with the actual situation.

Furthermore, by means of modelling and analyzing systematic error terms, the SLM-based method can also provide reference concerning the probable causes of machining errors in practical manufacturing and potential directions for improvement.

There are several possible directions for future research.

(1) In this study, only the circular and cylindrical profiles are taken as examples to study the monitoring process of geometric specifications with spatial correlations. The proposed method is general and can be utilized for other geometric specifications (e.g., free-form surfaces).
(2) Spatially correlated profile monitoring comprises challenging research that requires additional effort. This method provides reference for model-building of spatial correlation profiles and can be combined with other control charts such as exponentially weighted moving-average and cumulative sum control charts to detect small drifts in geometric specifications.
(3) This method can be extended to nonparametric profile monitoring with spatial correlations. When a profile is too complicated to be parameterized, the form of the parameter model can be replaced by a nonparametric form.

Declaration of Competing Interest

The authors declare that there are no conflicts of interest.

Acknowledgement

This work was supported by the National Natural Science Foundation of China (Grant No. 51775343) and sponsored by Shanghai Pujiang Program (Grant No. 18PJC031).

References

[1] Yan X, Ballu A. Tolerance analysis using skin model shapes and linear complementarity conditions. J Manuf Syst 2018;48:140–56.
[2] Zhang X, Wang X, Wang D, Wang X, Yao Z, Xi L. Methodology to improve the cylindricity of engine cylinder bore by honing. J Manuf Sci E-T ASME 2017;139(3):031008-031008-10.
[3] Shao Y, Yin Y, Du S, Xia T, Xi L. Leakage monitoring in static sealing interface based on three dimensional surface topography Indicator. J Manuf Sci E-T ASME 2018;140(10):101003.
[4] Deng CS, Chin JH. Hole roundness in deep-hole drilling as analysed by taguchi methods. Int J Adv Manuf Technol 2005;25(5–6):420–6.
[5] Keshteli RN, Kazemzadeh RB, Amiri A, Noorossana R. Functional process capability indices for circular profile. Qual Reliab Eng Int 2014;30(5):633–44.
[6] Kang L, Albin SL. On-line monitoring when the process yields a linear profile. J Qual Technol 2000;32(4):418–26.
[7] Zou C, Zhang Y, Wang Z. A control chart based on a change-point model for monitoring linear profiles. IIE Trans 2006;38(12):1093–103.
[8] Ding Y, Zeng L, Zhou S. Phase I analysis for monitoring nonlinear profles in manufacturing processes. J Qual Technol 2006;38(3):199–216.
[9] Williams JD, Woodall WH, Birch JB. Statistical monitoring of nonlinear product and process quality profiles. Qual Reliab Eng Int 2007;23(8):925–41.
[10] Kazemzadeh RB, Noorossana R, Amiri A. Phase i monitoring of polynomial profiles. Commun Stat-Theor M 2008;37(10):1671–86.
[11] Noorossana R, Eyvazian M, Vaghefi A. Phase ii monitoring of multivariate simple linear profiles. Comput Ind Eng 2010;58(4):563–70.
[12] Guo W, Shao C, Kim TH, Hu J, Jin J, Spicer P, et al. Online process monitoring with near-zero misdetection for ultrasonic welding of lithium-ion batteries: an integration of univariate and multivariate methods. J Manuf Syst 2016;38:141–50.
[13] Wang K, Jiang W, Li B. A spatial variable selection method for monitoring product surface. Int J Prod Res 2016;54(14):4161–81.
[14] Huang D, Du S, Li G, Zhao C, Deng Y. Detection and monitoring of defects on three-dimensional curved surfaces based on high-density point cloud data. Precis Eng 2018;53(7):79–95.
[15] Zou C, Qiu P, Hawkins D. Nonparametric control chart for monitoring profiles using change point formulation and adaptive smoothing. Stat Sinica 2008;19(3):1337–57.
[16] Zeng L, Neogi S, Zhou Q. Robust Phase I monitoring of profile data with application in low-E glass manufacturing processes. J Manuf Syst 2014;33(4):508–21.
[17] Yang W, Zou C, Wang Z. Nonparametric profile monitoring using dynamic probability control limits. Qual Reliab Eng Int 2017;33(5):1131–42.
[18] Wang H, Kababji H, Huang Q. Monitoring global and local variations in multichannel functional data for manufacturing processes. J Manuf Syst 2009;28(1):11–6.
[19] Cho N, Tu J. Roundness modeling of machined parts for tolerance analysis. Precis Eng 2001;25(1):35–47.
[20] Jiang Q, Feng HY, OuYang D, Desta MT. A roundness evaluation algorithm with reduced fitting uncertainty of CMM measurement data. J Manuf Syst 2006;25(3):184–95.

[21] Zhang XD, Zhang C, Wang B, Feng SC. Unified functional tolerancing approach for precision cylindrical components. Int J Prod Res 2005;43(1):25–47.
[22] Ramaswami H, Acharya SB, Kovvur Y, Anand S. A multivariate statistical analysis of sampling uncertainties in geometric and dimensional errors for circular features. J Manuf Syst 2006;25(2):77–94.
[23] Colosimo BM, Pacella M. On the use of principal component analysis to identify systematic patterns in roundness profiles. Qual Reliab Eng Int 2007;23(6):707–25.
[24] Pacella M, Colosimo BM. Multilinear principal component analysis for statistical modeling of cylindrical surfaces: a case study. Qual Technol Quant M 2016;15(4):1–19.
[25] Wang K, Li J, Tsung F. Registration-free monitoring of multimode near-circular shape profiles. Qual Reliab Eng Int 2018;34(4):529–42.
[26] Fathizadan S, Niaki STA, Noorossana R. Using independent component analysis to monitor 2-d geometric specifications. Qual Reliab Eng Int 2017;33(8):2075–87.
[27] Pacella M, Semeraro Q. Monitoring roundness profiles based on an unsupervised neural network algorithm. Comput Ind Eng 2011;60(4):677–89.
[28] Colosimo BM, Cicorella P, Pacella M, Blaco M. From profile to surface monitoring: spc for cylindrical surfaces via gaussian processes. J Qual Technol 2014;46(2):95–113.
[29] Liu JP, Jin R, Kong ZJ. Wafer quality monitoring using spatial dirichlet process based mixed-effect profile modeling scheme. J Manuf Syst 2018;48:21–32.
[30] Colosimo BM, Semeraro Q, Pacella M. Statistical process control for geometric specifications: on the monitoring of roundness profiles. J Qual Technol 2008;40(1):1–18.
[31] Solemani P, Noorossana R, Amiri A. Simple linear profiles monitoring in the presence of within profile autocorrelation. Comput Ind Eng 2009;57(3):1015–21.
[32] Yu JP, Liu JP. LR Prob control chart based on logistic Regression for monitoring mean shifts of auto-correlated manufacturing processes. Int J Prod Res 2011;49(8):2301–26.
[33] Anselin L. Spatial econometrics: methods and models. 1st ed Netherlands: Springer; 1988.
[34] Boeing commercial airplane group, quality assurance department. Advanced quality system tools. 2019 AQS D1-9000-1. http://www.boeingsuppliers.com/supplier/d1-9000-1.pdf [Accessed July 2018].
[35] Cliff A, Ord K. Testing for spatial autocorrelation among regression residuals. Geogr Anal 1972;4(3):267–84.
[36] Anselin L, Bera AK, Florax R, Yoon MJ. Simple diagnostic tests for spatial dependence. Reg Sci Urban Econ 1996;26(1):77–104.
[37] Breusch TS, Pagan AR. The lagrange multiplier test and its applications to model specifications in econometrics. Rev Econ Stud 1980;47(1):239–53.
[38] Damir MNH. Approximate harmonic models for roundness profiles. Wear 1979;57:217–25.
[39] Hii KF, Vallance RR, Grejda RD, Marshc ER. Error motion of a kinematic spindle. Precis Eng 2004;28(2):204–17.
[40] Ni W, Yao Z. Cylindricity modeling and tolerance analysis for cylindrical components. Int J Adv Manuf Technol 2013;64(5–8):867–74.
[41] Glenn P. Set of orthogonal surface error descriptors for near-cylinder optics. Opt Eng 1984;23:384–90.